journal

J. Am. Ceram. Soc., 1–6 (2011)
DOI: 10.1111/j.1551-2916.2011.04909.x

Factors Affecting Corrosion Resistance of Silicon Nitride Bonded Silicon Carbide Refractory Blocks

Ron Etzion[‡,†] and James B. Metson[§]

[‡]Light Metals Research Centre, University of Auckland, Auckland, New Zealand

[§]School of Chemical Sciences, University of Auckland, Auckland, New Zealand

The lifetime of aluminum reduction cells is driven primarily by the lifetimes of two components of the cell lining: the carbon cathode and the sidewall refractory material. The current state-of-the-art sidewall material is a silicon nitride bonded silicon carbide (SNBSC) refractory and its corrosion mechanisms in the aluminum reduction cell environment have been examined in this study. Microstructural analysis of commercial SNBSC materials identified variations in porosity and α/β Si_3N_4 ratio in the binder phase, with higher porosity levels and β Si_3N_4 content found in the interior part of the block. Unreacted metallic silicon was observed only as a crystalline phase encapsulated inside SiC grains and not in the binder phase. The effects on the corrosion rate of porosity levels, amount of binder, α/β Si_3N_4 ratio, and different factors in the environment, were examined in laboratory scale trials. High corrosion rates were associated with high porosity levels and a high β Si_3N_4 fraction in the binder. The crystal morphology of β Si_3N_4 is suggested as the main reason for the higher reactivity of this material. This morphology presents a higher surface area compared with α Si_3N_4 crystals. A corrosion mechanism for SNBSC materials in the aluminum reduction cell atmosphere is suggested.

I. Introduction

In modern high amperage aluminum reduction cells, the service life and the cell efficiency are strongly influenced by the life and condition of the cathode and of the sidewall refractory lining. The use of Si_3N_4 bonded SiC refractories has become the state of the art for sidewalls, and has largely replaced traditional carbon materials. The sidewall is typically protected by a frozen layer of the cryolite (Na_3AlF_6) electrolyte, but is periodically exposed to liquid electrolyte, to liquid aluminum, and to a range of vapor species in the cell gasses at temperatures approaching 1000°C.

The superior oxidation resistance, corrosion resistance, and thermal conductivity of silicon nitride bonded silicon carbide (SNBSC) materials compared with a carbon-based lining, has enabled the use of thinner cell linings giving increased cell capacity that can then accommodate larger anodes, higher amperage and hence, increased productivity.

Si_3N_4 bonded SiC materials are, however, still prone to oxidation and corrosion in the very aggressive environment of the aluminum reduction cell. Various parameters in the material properties such as porosity, amount of binder phase, presence of unreacted silicon or oxides, and α/β Si_3N_4 ratio, have been proposed to contribute to the enhanced corrosion rate.[1–3] The fact that these parameters are frequently interlinked makes it difficult to test each independently. However, some parameters were singled out as potentially having major contribution on the corrosion mechanism.

High open porosity can lead to the penetration of electrolyte and gaseous species into the material and thus, better contact with the bonding matrix. The typical porosity of the industrial materials is in the range 13–18% and the apparent density 2.6–2.7 g/cm^3. However, oxidation studies by Skybakmoen *et al.*[1] did not show a significant correlation between degree of corrosion and porosity.

The amount of the binder could also affect the corrosion resistance. Thermodynamically, Si_3N_4 is less stable than SiC in a cryolitic electrolyte and prone to oxidation by reaction with O_2 and CO_2 and reaction with corrosive gasses, such as HF and $NaAlF_4$, which are emitted during cell operation.[3–6] A balance should be maintained in the binder content; low binder content will reduce bath penetration and corrosion, however, it will also reduce the strength of the material. Increased binder content will provide a stronger material, but will potentially expose the material to a higher degree of corrosion.

Oxides, such as alumina and silica, are typically added as sintering aids for production of higher strength refractory materials,[7,8] however, for these materials, the presence of oxides showed negative effect on the resistance of the material to corrosion by cryolite.[9] Oxide bonded refractory materials based on SiO_2, Mullite, clay and alumina, which employ a low melting point phase, have been found unsuitable to withstand the corrosive environment in the aluminum reduction cell.[10–12]

Despite significant improvements in refractory quality, there is still considerable uncertainty over the factors, which limit the life of these SNBSC refractories, coupled with a tendency for precipitous failure. Thus, there is considerable interest in better understanding these failure mechanisms.

II. Experimental Procedure

(1) Microstructure Analysis

Microstructural analysis of SNBSC samples from eight different pristine blocks from various manufacturers (denoted blocks A-G) was obtained using techniques such as X-ray diffraction (XRD), SEM-EDS, and solid state NMR. The blocks varied in cross-section between 75 and 100 mm in width, although the internal microstructures were visually similar.

Powder XRD analysis was performed on crushed samples from different SNBSC blocks to quantify the α and β Si_3N_4 content of the binder phase, using the method of Gazzara & Messier.[13] The powder XRD patterns were acquired using Bruker D8 Avance diffractometer operated at 40 kV and 40 mA, using Cu$K\alpha$ radiation and a KF crystal monochromator.

The SNBSC samples were also analyzed using solid state NMR, which was used as a complementary method to XRD

M. Rigaud—contributing editor

Manuscript No. 29757. Received May 29, 2011; approved September 19, 2011.
†Author to whom correspondence should be addressed. e-mail: r.etzion@auckland.ac.nz

analysis due to its ability to detect both crystalline and noncrystalline phases not detected by XRD analysis. This method is useful in detection of any amorphous Si that could be formed due to freezing of a molten silicon phase. A Bruker AVANCE 300 spectrometer operating at 300.13 MHz proton frequency and at 59.63 MHz silicon frequency was used for all solid-state NMR experiments. The basic spectra were obtained using "standard" one-pulse-and-collect experiments.

A scanning electron microscope (SEM) equipped with an energy dispersive X-ray (EDX) was used to study the material morphology, using its ability to provide high magnification imaging (4000× to 16 000×) enabling the observation of the distribution of different phases within the material, the crystal shape, and arrangement of the different phases.

A FEI Quanta 200F field-emission SEM operating at 20 kV electron energy was used, with a spot setting of 4.0, as high magnification (4000× to 16 000×) imaging tool with either a secondary electron detector or a backscattered electron detector.

Porosity measurements were performed on segments taken along an SNBSC brick cross-section using the ISO 5017 standard method based on the Archimedes principle.

(2) Corrosion Testing Methodology

The corrosion testing was carried out in two stages: in the first stage four samples (size 15 × 15 × 165 mm) were placed symmetrically in a graphite crucible (internal diameter 120 mm with 190 mm depth) filled with 8 cm of a molten electrolyte (bath) with a composition of 78% cryolite (high purity, Central Glass Co, Ube, Japan), 7% alumina (smelter grade), 10% AlF_3 (smelter grade), and 5% CaF_2 (high purity, Riedel de haën, Seelze, Germany) and partly immersed in the molten bath. After 48 h of soaking at 1000°C, the samples were taken out and cooled, the adhering bath was removed from the impregnated samples using knife after soaking in aluminum chloride solution (to loosen the adhering bath) in an ultrasonic bath. The sample volume, density, and porosity were measured before and after the immersion using the ISO 5017 standard method.

The second stage is a 48 h polarized corrosion test, which is performed in an experimental rig (Fig. 1) based on the method developed by Skybakmoen *et al.*[4] The arrangement is important, because it simulates the cell gasses and electrolyte movement to which refractories are exposed during cell operation. The clean, dry impregnated samples were placed back in the molten bath, and a constant current of 15 A was passed through the electrolyte that was kept at 1000°C. A graphite cylinder (30 mm in diameter) screwed into a threaded stainless steel rod served as an anode, while the graphite crucible wall, connected to the power supply by a threaded stainless steel rod, served as the cathode. The anode was rotated by an electric motor and the current was passed to the anode support rod via a carbon brush. Rotation was maintained to ensure electrolyte movement and gas distribution, to stabilize the voltage and to avoid short circuits due to carbon dust build up on the electrolyte surface between the crucible wall and the anode.

The cell operating voltage was maintained in the range 3.5 –4.2 V during the experiment, while a mixture of alumina and cryolite (60/80 g, respectively) was fed into the bath periodically and the graphite anode was replaced after 24 h. The current, voltage, and bath temperature were monitored and recorded using data logger, the anode circumference and length change were measured to ensure consistency of the cell conditions. The SNBSC samples volume change between the pre and post polarized test serves as an indication for the corrosion resistance of the materials; during the test the binder phase is attacked by corrosive gasses such as HF and $NaAlF_4$ to produce volatile SiF_4 which corrode the material, and lead to reduction in its volume. Due to infiltration of bath, the weight change cannot be used as a measure of corrosion.

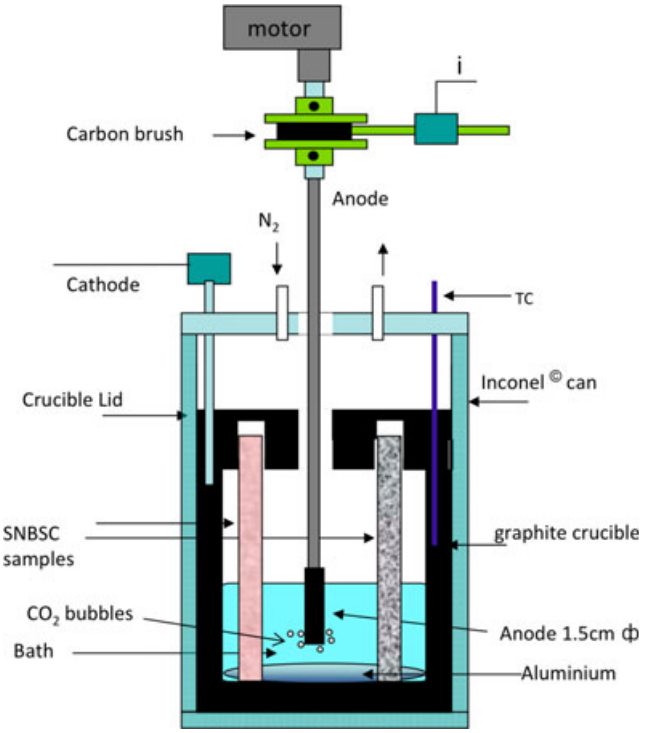

Fig. 1. The polarized corrosion-testing rig.

III. Results

(1) Morphology

Variations in morphologies of the different silicon nitride phases in the bonding phase are clearly revealed in SEM observations at high magnification. Three main crystal types were observed in the silicon nitride bonding-phase: The first type has long fine needle-like crystals with high surface area and an aspect ratio >25 which were observed in limited areas and only within the pores [Fig. 2(a)]. This type of fine needle-like crystals is associated with a polymorph of α Si_3N_4 as described by Wang[14] and Jennings *et al.*[15] who observed them at formation temperatures between 1350°C and 1400°C. The second type of crystal morphology is a flat, matte-like crystal [Fig. 2(b)], which was observed in samples with a high α Si_3N_4 content (as measured using XRD).

The third type of crystals, observed in samples with high β Si_3N_4 content, has an elongated shape, with distinctively hexagonal cross-section [Fig. 2(c)]. This crystal morphology for β Si_3N_4 is well documented in the literature.[15–19] Analysis of cross-sections of corroded SNBSC samples cut above the bath line showed enhanced porosity and cavities with SiC in the center at the exterior face, and reduced porosity in the core, filled with sodium and fluoride rich species.

(2) Free Si as a Contributor to Corrosion Rate

The high reactivity of silicon in fluoride environments suggests the hypothesis that the corrosion rate of SNBSC materials in the aluminum reduction cell atmosphere could be related to the free silicon content and its distribution within the SNBSC bonding phase. The free Si arises from incomplete reaction of the binder phase precursor due to formation of Si liquid during the fabrication of the block when temperatures in excess of 1400°C are being reached in the interior bulk during formation of the Si_3N_4 bond phase. Any Si freezing from the liquid phase will be difficult to convert to the Si_3N_4 bond phase due to the low surface area and thus slow kinetics of this reaction.

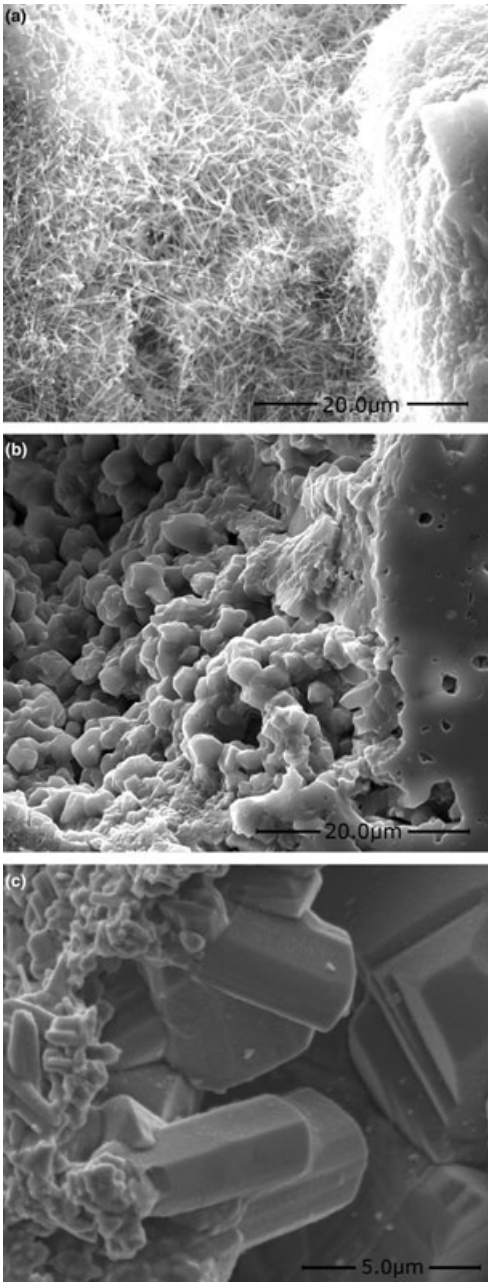

Fig. 2. SEM micrograph of long, fine α Si_3N_4 crystals growing into a pore in an SNBSC sample (A) flat-matte shaped α Si_3N_4 crystals in the bonding phase (B). SNBSC bonding phase material with long hexagonal β Si_3N_4 crystals (C)

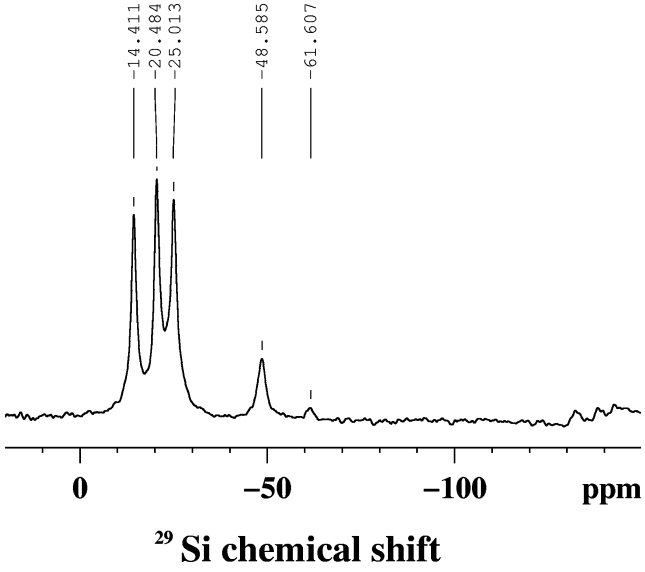

Fig. 3. Solid state NMR of SNBSC sample showing the presence of SiC (peaks at −14.41, −20.48, −25.0 ppm) Si_3N_4 (peak at −48.58 ppm) and Si_2N_2O (peak at −61.60 ppm) with absence of free Si (peaks around −100 ppm).

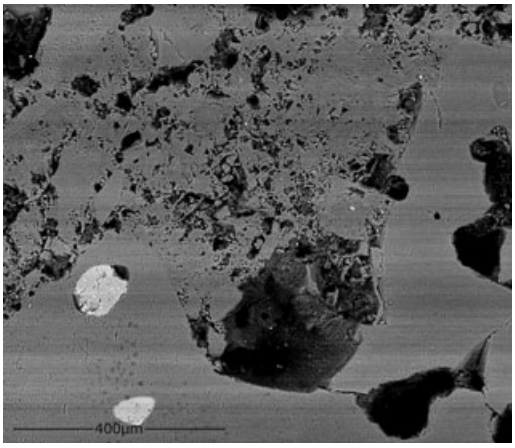

Fig. 4. Back scattered electron SEM images of SNBSC samples depicting free Si in the core of the SiC grains (lighter colored spots) and not in the bonding matrix

However, only low residual free Si is observed in Analytical XRD results on numerous SNBSC samples, with maximum content ~7% in isolated cases. Si concentration was higher in samples taken from the interior part of the bricks and was usually accompanied by higher β Si_3N_4 concentration.

To detect any amorphous Si that could be formed due to freezing of a molten silicon phase, the SNBSC samples were also analyzed by Solid State NMR which can detect both crystalline and noncrystalline phases that cannot be detected using XRD analysis. The results (Fig. 3) confirmed that all the phases found in the samples were crystalline, including the free silicon concentration, which was minimal.

SEM-EDS analysis of a large number of samples from various bricks indicates that the free Si was mainly observed in the core of SiC grains and not in the Si_3N_4 bonding matrix. This indicates that the source of free silicon is unreacted silicon from the SiC production process and not from the production of silicon nitride. The free Si was easily observed when using a back-scattered electron detector, and appeared white compared with the gray SiC grain or Si_3N_4 phases (Fig. 4). This suggests that free Si has a minimal role in determining corrosion resistance in these materials.

(3) Variation of Porosity Level

Porosity measurements show variation with position (seen in Fig. 5), with higher porosity usually observed in the interior areas. In some bricks, the porosity levels of segments taken from the exterior area of one face of each brick were higher than those taken from segments of the exterior part of the opposite face. The difference in the porosity between the two exterior parts may be due to differential exposure to nitrogen gas flow during nitridation because of the stacking arrangement of the bricks in the furnace.

(4) α and β Si_3N_4 Distribution

As discussed above, SNBSC materials contain both α and β Si_3N_4 phases in a ratio, which varies in blocks from different manufacturers. Samples taken from the exterior and the interior area of a cross-section slice of each brick showed an

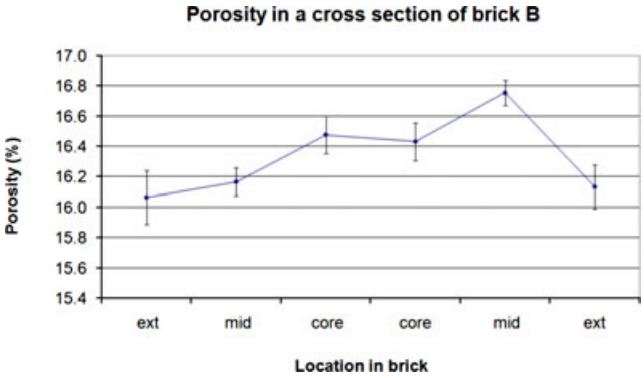

Fig. 5. Porosity of segments cut along a cross-section of SNBSC brick.

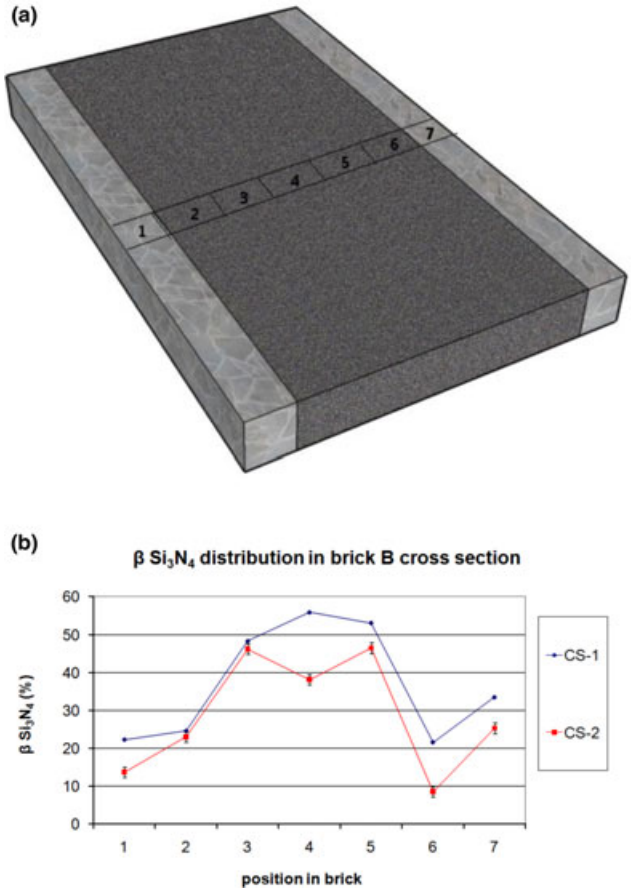

Fig. 6. (a) Schematic diagram of SNBSC block cross-section with locations numbered one to seven of analyzed samples. (b) β Si_3N_4 content in the binder measured on samples that were cut along two cross-sections (locations 1–7) taken from brick B.

uneven distribution of α and β Si_3N_4 content. Higher β Si_3N_4 content was usually observed in the interior part of the brick as seen in Fig. 6

The high β Si_3N_4 content observed in the internal area of some bricks is probably attributed to high temperatures during the nitridation stage of the fabrication process. The excess heat generated during the exothermic nitridation reaction is dissipated more easily from the exterior part of the brick than from the interior, as calculated in steady-state thermal modeling.[20] Temperatures above 1500°C and the presence of a molten liquid silicon in the interior zone creates conditions which can enhance the conversion from α to β Si_3N_4 resulting in higher β Si_3N_4 content in the interior of the brick.

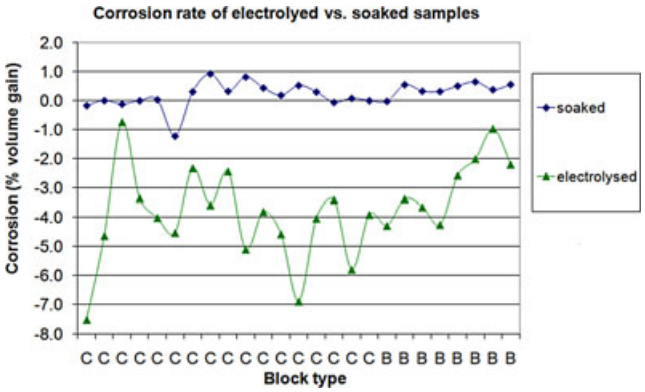

Fig. 7. Comparison between corrosion rates of samples exposed to bath alone and to exposure under electrolysis conditions. The block type refers to samples cut from block B or block C.

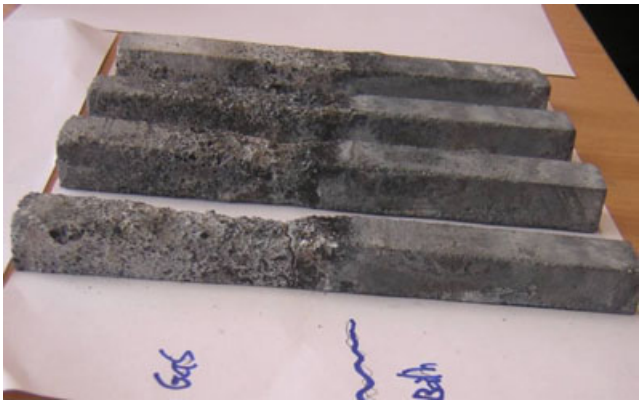

Fig. 8. SNBSC samples (25 × 20 × 185 mm^3) after exposure to 48 h corrosion testing. Degradation of the samples is observed mainly at the bath-gas interface and in the gas phase.

Oxide phases such as Si_2N_2O and SiO_2 were also detected using XRD analysis in a few of the samples tested, especially in the core of the blocks. The concentration of Si_2N_2O was between 1% and 3% with extreme cases above 5%, SiO_2 was detected only at locations within three samples.

(5) Corrosion Results

Thermodynamically, the potential for the SNBSC materials to act directly with the cryolitic bath is minimal due to the positive Gibbs free energies (ΔG = 500 kJ/mole) of the reactions of Si_3N_4 and SiC with cryolite. The corrosion rates of samples that were only soaked in bath were compared with the corrosion rates of these samples after additional exposure to polarized corrosion testing. The exterior surface of most of the samples that were only soaked in bath was largely undamaged and their corrosion rates were much lower compared with the samples that were exposed to the polarized corrosion test (Fig. 7). Corroded samples after polarized testing showed degradation mainly in the area exposed to the cell gas, while the part immersed in the electrolyte bath stayed intact (Fig. 8).

Following the observation that SNBSC samples are corroded mainly above the bath line, an experiment was performed to verify whether the corrosive and oxidative gasses are the only contributors to SNBSC degradation in the cell atmosphere, or whether the penetrated bath has an active role in this process. Pristine SNBSC samples that were placed above the bath during electrolysis showed little corrosion; however, when these samples were soaked in the bath for 48 h and then reposition in the gas atmosphere above the bath level for a further 48 h, intensive degradation was observed, as seen in Table I.

Table I. Corrosion Rate of SNBSC Samples Following Exposure to Only the Gas Phase, and After 48 h of Bath Immersion

Samples	D1	D2
Porosity [%]	13.6 ± 0.4	15.6 ± 0.6
Corrosion in exposure to only gas phase for 36 h [% volume gain]	+0.4	+0.4
Corrosion in exposure to only gas phase for additional 96 h [% volume gain]	−1.0 ± 0.7	−0.9 ± 1.0
Corrosion after 48 h exposure to gas phase post 48 h bath soak [% volume gain]	−8.48 ± 0.07	−11.61 ± 0.07

The corrosion rates of samples that were soaked in bath for 48 h and then exposed to electrolytic conditions for 48 h were measured as a function of their porosity levels. The corrosion rate is expressed as percentage of volume gain and is shown in Fig. 9. A linear regression curve fitted to the corrosion results shows that there is a measurable correlation between the porosity and the corrosion rate of the SNBSC samples. The coefficient of determination (R^2) of 0.43 indicates some correlation between the higher corrosion rate and higher porosity.

Thermodynamic calculations suggest that the binder phase of the SNBSC blocks, rather than the SiC phase, is prone to attack by oxidizing agents (CO, CO_2, and O_2) and corrosive gasses (HF and $NaAlF_4$) present in the aluminum reduction cell atmosphere.[21] Hence, to verify these calculations, the corrosion rates of the samples tested in the lab-scale corrosion test were presented as a function of their SiC content (which was measured using XRD analysis). The data suggest reasonably consistent behavior of reduced corrosion rate with increased SiC content up to an SiC content of around 80%. Despite the scatter, which is expected for these relatively complex composite materials, higher and more variable corrosion rates are observed in samples particularly when the SiC content exceeds around 80%.

(6) Effect of α/β Si_3N_4 Ratio on the Corrosion Rate of SNBSC Bricks

The binder phase contains mainly α and β Si_3N_4, low concentrations of oxides (Si_2N_2O and SiO_2) and, in some cases, unreacted Si. Given that the binder is more reactive than the SiC matrix, it is then worth examining the influence of different phase compositions in the binder itself. The corrosion rate of the presoaked samples was thus measured as a function of their β Si_3N_4 content. A positive, correlation between the corrosion rate and β Si_3N_4 content was observed (Fig. 10).

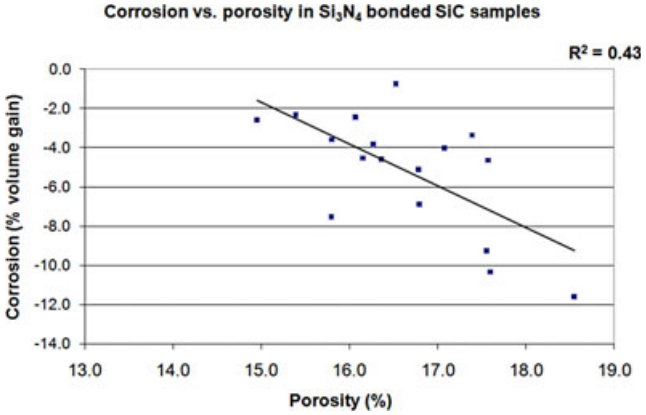

Fig. 9. Corrosion rate (measured as% volume gain) of SNBSC samples as a function of porosity levels.

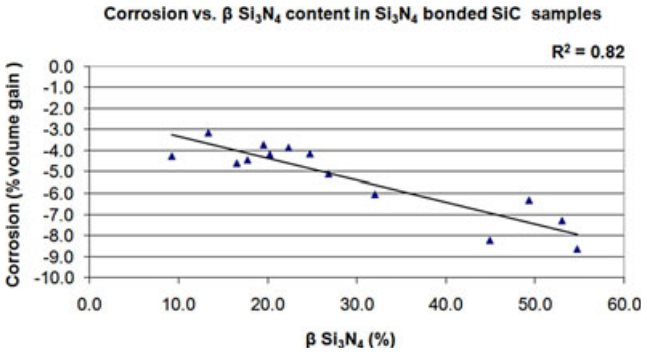

Fig. 10. Corrosion rate as a function of β Si_3N_4 content of SNBSC samples. High correlation was found between the corrosion rate and β Si_3N_4 content with calculated $R^2 = 0.82$.

(7) Effect of Surface Area and Pore Size Distribution

The surface area and the pore size distribution were determined for samples from each block using standard nitrogen adsorption techniques. The BET surface area of pristine blocks that were tested was low in the range 0.10–0.35 m^2/g, and the absolute accuracy of the measurements is questionable, however, the low surface area suggest that the effect of the surface area on the corrosion rate is likely to be minimal. The pore size distribution analysis (based on BJH Adsorption) indicates that the total volume of pores with radius below 300 nm is negligible, hence, it is concluded that the majority of the porosity lay in the macro range.

IV. Discussion

Porosity measurements conducted on segments taken along an SNBSC block cross-section showed variation with position. However, the nature of this variation is different for particular blocks. Higher porosity in the interior areas was observed in some of the blocks tested, while other blocks did not show large variations in porosity levels between the exterior and the interior parts.

The corrosion rates of the SNBSC samples were measured as a function of their porosity. Samples that were soaked for 48 h in a cryolitic bath prior to the corrosion test showed some correlation between the corrosion rate and their porosity levels. The calculated coefficient of determination (R^2) indicates that only 43% of the variability of the corrosion rate results can be explained by the variations in porosity levels. The effect of the sample width on the correlation between corrosion rate and porosity is profound. Thicker samples with widths above 16 mm showed no measureable correlation between the corrosion rate and porosity, suggesting the inhomogeneous nature of the samples (in binder phase composition) and that electrolyte penetration is limited in the pore size range these samples exhibit.

Samples with a significant difference in porosity levels, taken both from the same brick, and from two different bricks that were tested in the same experiment, showed significantly higher corrosion rates for the higher porosity samples.

The corrosion rate of SNBSC samples was also measured as a function of their SiC content. Despite the scatter in the data, the corrosion results of the presoaked samples in electrolyte showed an optimal SiC content in terms of corrosion resistance. The minimum corrosion rate was observed in samples having 80–85% SiC, while above this range increasing and increasingly scattered corrosion levels are observed. This is presumably attributed to increased reactivity where the binder content is high and the lack of sufficient binder phase to provide a dense and coherent binder matrix when the binder content is low.

The influence on the corrosion rate of the distribution of α and β Si_3N_4 phases found in the binder was examined. These two phases are not evenly distributed in the SNBSC blocks,

as segments cut along the central cross-section of different blocks showed variations in β Si_3N_4 content with an increase of the β Si_3N_4 content when moving from the exterior part of the brick to the core. A high correlation between corrosion rates and high β Si_3N_4 content in sample was observed with $R^2 = 0.82$. The crystal morphology of β Si_3N_4 is suggested as the reason for the high reactivity of these materials. This morphology is characterized by elongated rod-shaped crystals with hexagonal cross-section, presents a higher surface area compared with the flat, matte-like α Si_3N_4 crystals. Thus, they are more reactive due to their high aspect ratio of exterior surface area versus volume that is exposed to the corrosive gas attack. The fine needle-like α Si_3N_4 crystals with the highest aspect ratio would be expected to be more prone to attack, but were only observed in a few isolated pores, hence, are not expected to have a major impact on degradation of the block. As in the porosity trials, samples wider than 16 mm showed low correlation due to inaccessible porosity and the incorporation of zones with different β Si_3N_4 content within the sample.

Although much more corrosion was observed in the part of the sample exposed in the gas zone than that immersed in the bath, the contribution of the penetrated bath is significant. Exposure of SNBSC samples to only the gas phase showed very limited corrosion over the longer period of exposure (96 h). This is probably due to formation of a protective layer of SiO_2 as a result of oxidation of SiC and Si_3N_4 by CO_2 that inhibits degradation by corrosive gasses, such as HF and $NaAlF_4$. Exposure of the oxidized samples to the cryolitic bath resulted in enhanced degradation caused by dissolution and removal of the protective SiO_2 layer and oxidation of the more reactive binder phase to sodium silicates aided by attack by the penetrated sodium. The higher reactivity of sodium silicate toward corrosive gasses, compared with SiC, Si_3N_4 phases,[14,21–23] and the exposure of the entire samples surface area to the corrosive environment, led to extensive degradation. This observation also explains the contribution of higher porosity on the degradation of SNBSC samples.

Based on the corrosion results of the presoaked SNBSC samples, a multivariate regression statistical model was built which identified porosity levels, β Si_3N_4 content, (β Si_3N_4 content),[2] and SiC content × β Si_3N_4 content as factors that show a statistically significant correlation to the corrosion rate. The relative contribution of each factor is expressed by the respective regression coefficients. A regression equation [Eq. (1)] with coefficient of determination of 0.7 was made based on the contributing factors and their coefficients, that estimates corrosion rate for a given porosity level, β Si_3N_4 content, and SiC content.

$$\begin{aligned}\text{Corrosion rate} = {} & 38.86 - \text{porosity level } (\%) \\ & - 0.973\ \beta\ Si_3N_4 \text{ content } (\%) \\ & - 0.35\text{SiC content } (\%) \\ & - 0.0042\ (\beta\ Si_3N_4 \text{ content})^2 \\ & + 0.015\ (\beta\ Si_3N_4 \text{ content} \times \text{SiC content})\end{aligned} \quad (1)$$

The largest single factor affecting corrosion appears to be porosity levels. However, β Si_3N_4 content in the binder, and the binder:SiC ratio, also show significant contributions.

V. Conclusions

The microstructure of SNBSC refractories was studied to understand the impact on the corrosion mechanism in aluminum reduction cell environments. Industrial SNBSC samples that were tested in lab-scale corrosion tests showed that porosity levels and β Si_3N_4 content make a statistically significant contribution to the corrosion rate. Higher corrosion rates were related to high porosity levels and/or high β Si_3N_4 content. The unique morphology of β Si_3N_4 crystals with higher surface area is proposed to lead to higher reactivity.

The amount of binder was also identified as a statistically significant contributor to the corrosion rate of the SNBSC samples, with minimum corrosion occurring in samples with 80–85% SiC content. Unreacted silicon was found only within SiC grains and not in the binder phase, hence, was excluded as a parameter that contributes to the corrosion rate.

Corrosion was observed mainly in the gas phase and especially at the bath-gas phase interface, however, corrosion appears to be driven by the combined effect of bath penetration into the porous SNBSC material, and exposure to the corrosive gasses.

References

[1]E. Skybakmoen, H. Stoen, J. H. Kvello, and O. Darell, "Quality Evaluation of Nitride Bonded Silicon Carbide Sidelining Materials"; pp. 773–8 in *Light Metals*, Edited by H. Kvande. TMS, Warrendale, PA. San Francisco, CA, 2005.

[2]E. Skybakmoen, J. Kvello, O. Darell, and H. Gudbrandsen, "Test and Analysis of Nitride Bonded SiC Sidelining Materials: Typical Properties Analysed 1997–2007"; pp. 943–8 in *Light Metals*, Edited by D. H. De Young. TMS, Warrendale, PA. New Orleans, LA, 2008.

[3]F. B. Andersen, G. Dörsam, M. Stam, and M. Spreij, "Wear of Silicon Nitride Bonded SiC Bricks in Aluminium Electrolysis Cells"; pp. 413–8 in *Light Metals*, Edited by A. Tabereaux. TMS, Warrendale, PA. Charlotte, NC, 2004.

[4]E. Skybakmoen, H. Gudbrandsen, and L. I. Stoen, "Chemical Resistance of Sideline Materials Based on SiC and Carbon in Cryolitic Melts – A Laboratory Study"; pp. 215–22 in *Light Metals*, Edited by C. Edward Eckert. TMS, Warrendale, PA. San Diego, CA, 1999.

[5]M. Thorley and R. Banks, "Kinetic and Mechanism of Oxidation of Silicon Nitride Bonded Silicon Carbide Ceramic," *J. Therm. Anal.*, **42**, 811–22 (1994).

[6]M. V. Swain and E. R. Segnit, "Reaction Between Cryolite and Silicon Carbide Refractories," *J. Austr. Ceram. Soc.*, **20**, 9–12 (1984).

[7]D. P. Edwards, B. C. Muddle, Y. B. Cheng, and R. H. J. Hannink, "The Development of Microstructure in Silicon Nitride-Bonded Silicon Carbide," *J. Eur. Ceram. Soc.*, **15**, 415–24 (1995).

[8]D. R. Messier, F. L. Riley, and R. J. Brook, "The α/β Silicon Nitride Phase Transformation," *J. Mater. Sci.*, **13**, 1199–205 (1978).

[9]J. Zhao and Z. Cheng, Comparison of Cryolite Resistance of Silicon Carbide Materials.in7th Australasian Aluminium Smelting Technology Conference and Workshop, Nov 11–16. University of New South Wales, Melbourne, Australia, 43–9, 2001.

[10]D. John and R. Maurage, "Sialon Bonded Silicon Carbide Sidewall Pieces for the Aluminium Reduction Cell," *Ceram. Ind. int.*, **182** [182] 42 (1992).

[11]A. F. Fickel, J. S. Kramass, and P. Temme, "Silicon Carbide Refractories for Aluminum Reduction Cell Linings"; pp. 183–8 in *Light Metals*, Edited by R. D. Zaberznick. TMS, Warrendale, PA. Denver, CO, 1987.

[12]A. T. Tabereaux and A. Fickel, "Evaluation of Silicon Carbide Bricks"; pp. 483–91 in *Light Metals*, Edited by U. Mannweiler. TMS, Warrendale, PA. San Francisco, CA, 1994.

[13]C. P. Gazzara and D. R. Messier, "Determination of Phase Content of Si_3N_4 by X-Ray Diffraction Analysis," *Bull. Amer. Ceram. Soc.*, **56** [9] 777–80 (1977).

[14]Zhaohui Wang, Egil Skybakmoen, and T. Grande, "Chemical Degradation of Si_3N_4-Bonded SiC Sidelining Materials in Aluminum Electrolysis Cells," *J. Am. Ceram. Soc.*, **92** [6] 1296–302 (2009).

[15]H. M. Jennings and M. H. Richman, "Structure, Formation Mechanisms and Kinetics of Reaction-Bonded Silicon Nitride," *J. Mater. Sci.*, **11**, 2087–98 (1976).

[16]H. Björklund, J. Wasen, and L. K. L. Falk, "Quantitative Microscopy of β Si_3N_4 Ceramics," *J. Am. Ceram. Soc.*, **80** [12] 3061–9 (1997).

[17]H. Björklund and L. K. L. Falk, "β-Si_3N_4 Grain Growth, Part II: Intergranular Glass Chemistry," *J. Eur. Ceram. Soc.*, **17** [11] 1301 (1997).

[18]H. Björklund, L. K. L. Falk, K. Rundgrenb, and J. Wasénc, "β-Si_3N_4 Grain Growth, Part I: Effect of Metal Oxide Sintering Additives," *J. Eur. Ceram. Soc.*, **17** [11] 1285 (1997).

[19]F. F Lange, "Strong, High-Temperature Ceramics," *Annu. Rev. Mater. Sci.*, **4**, 365–90 (1974).

[20]R. Etzion, J. B. Metson, and N. Depree, "Wear Mechanism Study of Silicon Nitride Bonded Silicon Carbide Refractory Materials"; pp. 955–9 in *Light Metals*, Edited by D. H. De Young. TMS, Warrendale, PA. New Orleans, LA, 2008.

[21]R. Etzion, *Degradation Mechanisms and Development of Silicon Carbide Refractories, in Chemistry*. University of Auckland, Auckland, 2008.

[22]T. Sun, G. R. Pickrell, and J. J. Browen, "Corrosion Kinetics of Silicon Nitride in Dry Air Containing Sodium Nitrate Vapors," *J. Am. Ceram. Soc.*, **77** [12] 3209–14 (1994).

[23]M. I. Mayer and F. L. Riley, "Sodium-Assisted Oxidation of Reaction-Bonded Silicon Nitride," *J. Mater. Sci.*, **13**, 1319–28 (1978). □